https://science.utm.my/procscimath
Volume 24 (2024) 33-46

Propagation of Internal Gravity Waves Above Topography

Eu Pei Qi, Muhamad Najib Zakaria
Department of Mathematical Sciences, Faculty of Science, Universiti Teknologi Malaysia
Corresponding author : mnajibz@utm.my

Abstract
Internal gravity waves play a vital role in shaping the dynamics of both Earth's atmosphere and ocean, which can influence the circulation patterns and mixing processes. A significant research gap persists in understanding how these waves propagate in the presence of topographic features. The purpose of this study is to investigate the behaviour of internal gravity waves as they interact with hills. The mathematical model considers motion in both x and z directions, accounting for a uniform background horizontal wind speed. Three distinct cases are investigated, which are case 1 : $N^2 = k^2U^2$; case 2 : $N^2 < k^2U^2$; and case 3 : $N^2 > k^2U^2$. The methods of direct integration and characteristic function are employed to solve the differential equations. The physical quantities of waves, including velocity, pressure, and density are visualized using MATLAB software by using different values of horizontal wavenumber. The results showed that a shorter wavenumber corresponds to a higher wavelength and lower frequency. In case 3, the waves have zero frequency but have group velocity. It is observed that the waves maintain a consistent energy transfer during propagation. In conclusion, variations in horizontal wavenumber have significant impact on the behaviour of internal gravity waves when they propagate above topography.
Keywords: internal gravity waves; topographic features; mathematical model; partial differential equations; horizontal wavenumber

1. Introduction

Internal gravity waves are waves that oscillate within a fluid medium, which caused by variations in density. German glider pilots have discovered the existence of mountain waves, which are one of the types of internal gravity waves [1]. The presence of mountain waves have the relation with the high-altitude clouds [2]. Before the investigation of internal gravity waves, there is a need to derive the mathematical model. Lteif and Khorbatly [3] have presented the derivation and mathematical analysis of the model of internal gravity waves. The internal gravity waves are mainly investigated on its characteristics. Durran mentioned that the characteristics of internal gravity waves are related with linear theory [4]. The behaviour of internal gravity waves depend on the observation of the time scale [5]. The waves' behaviour are simulated using Fast Fourier transform and the results showed that not all waves have the same propagation speed [6]. Previous study also revealed that an increase in wind results in a decrease in vertical wavelength [7].

The investigation on the wave propagation used Boussinesq approximation as it is a key tool for the analysis of internal gravity waves. Many researchers have employed the Boussinesq approximation in their research, especially investigating on lee wave phenomena [8]. The equations of internal gravity waves have been solved by involving Boussinesq approximation [9,10]. By using Boussinesq approximation, the nonlinear Boussinesq-type model can be derived [11] and the characteristics of nonlinear internal gravity waves can be analysed [12]. Besides, Charlier and Lenells [13] also established Boussinesq approximation in determining the solutions with the implementation of Inverse Scattering Transform (IST) for the initial value problem.

Furthermore, the analysis of the solutions related to energy of internal gravity waves is crucial in the field of wave dynamics. Eden et al. [14] investigated the mechanism of energy transfer of internal gravity waves using numerical simulation. They have evaluated the kinetic energy using three different

methods, while the potential energy has been analysed by other researchers [15]. According to [16,17],

the researchers also examined the energy produced by internal gravity waves. The rotary spectral the researchers also examined the energy produced by internal gravity waves. The rotary spectral analysis is used in investigation of energy distribution [18]. Khatiwala [19] also investigated on the generation of energy under the influence of bottom topography. The findings showed that a sizable topographic features significantly reduced the rate of energy transfer. Not only that, the researchers also have discussed on the energy density above the wave peak [20]. The energy density of internal gravity waves is larger when the buoyancy frequency is higher [21].

When investigating the internal gravity waves, several numerical methods have been used by the researchers, such as Finite Difference Method (FDM), Finite Element Method (FEM), and Finite Volume Method (FVM). FDM is the most common method used in simulations of internal gravity waves. The researchers have used second order finite difference scheme in discretization the partial differential equation of internal gravity waves [22]. Two-dimensional equations have been solved using FDM [23-25]. Shi et al. [26] solved the nonlinear Boussinesq model for surface gravity waves using FDM, while Johnston and Merrifield [27] used FDM to solve Princeton Ocean Model (POM). Besides, Rizal et al. [28] analysed the response of internal gravity waves in finite channel using FDM and the results showed that variations in amplitudes and periods contributes to variations in the signal of internal gravity waves time-series. On the other hand, three-dimensional flow problems have been solved using FEM by the researchers [29,30]. A scaled boundary finite element method (SBFEM) has been employed in [31]. Previous studies also revealed that the use of FEM can approximate the data generating process [32] and determine the accuracy and convergence of the model [33]. Moreover, the simulation of internal gravity waves are done through the employment of FVM with the combination of other method, model or algorithm [34-37]. For example, the researchers have presented FVM on solving nonhydrostatic Navier-Stokes equations with the Bossinesq model [38].

Moreover, several laboratory experiments have conducted by researchers in order to detect the changes of the behaviour of internal gravity waves. Matsuura and Hibiya [39] have did the experiments on the generation of internal waves due to the interaction of tides and topography. They observed the vertical density stratification with constant temperature gradient. The experiments by Lim et al. [40] also investigated on the generation of waves and they reported the waves occurred within the finite length of slope about the critical point. The laboratory experiments on the behaviour of wave propagation also investigated and analysed in [41,42]. The researchers in [43,44] have did the laboratory experiments to observe the internal wave attractors, while the researchers in [45] did the laboratory experiments to observe the stream function field. Additionally, many researchers have conducted numerical simulations of internal gravity waves. Klemp and Lilly [46] developed two-dimensional numerical model to simulate internal gravity waves with finite amplitude, while Xu et al. [47] investigated on the waves generated in directional wind over idealized terrain. The numerical experiments also conducted to analyse the propagation of internal gravity waves [48-50]. The researchers reported the numerical simulations of internal wave reflection in the bottom boundary layer over sloping topography [51]. Other numerical simulations of waves can be found in [52-56].

The main purpose of this study is to provide valuable insights and findings regarding the behaviour of internal gravity waves when they propagate above the topography. In this study, three distinct cases are investigated in which the horizontal wavenumber used are vary. The aim of this study is to compare the values of physical quantities as horizontal wavenumber vary. This paper is structured as follows. The methodology consists of mathematical formulation of internal gravity waves are outlined in Section 2. Section 3 presents analytical solutions to the second order ordinary differential equation for three distinct cases. The results of the behaviour of internal gravity waves above topography are discussed in Section 4. The last section contains conclusion and recommendations for future research work.

2. Methodology

In order to analyse the behaviour of internal gravity waves under the influence of topography, the first thing is to derive the equation governing internal gravity waves within the Boussinesq approximation

incorporating the effects of a uniform horizontal wind speed. Subsequently, the mathematical model is modified to include the presence of topographic features during the propagation of internal gravity waves.

2.1 Mathematical Formulation in Horizontal Flow

Consider the fluid flow is incompressible and the flow density remains constant at time, t. The fluid flow problem follows the fundamental physical principle of mass is conserves and momentum is conserves, which yields the equations below.

$$\frac{\partial \mathbf{u}}{\partial t} + (\mathbf{u} \cdot \nabla)\mathbf{u} = -\frac{1}{\bar{\rho}}\nabla p - \frac{\rho g}{\bar{\rho}}\mathbf{e}_z + \mathbf{D} \tag{1}$$

$$\nabla \cdot \mathbf{u} = 0 \tag{2}$$

$$\frac{\partial \rho}{\partial t} + \mathbf{u} \cdot \nabla \rho = 0 \tag{3}$$

where $\mathbf{u}$ is velocity of fluid, ∇ is gradient, ρ is density of fluid, p is pressure, and $\mathbf{F}$ is forces on the fluid.

Internal gravity waves can be find in ocean where the density is vary depends on the height. By assuming that the variations in the density is no more than $\pm 2\%$ from the average density, $\bar{\rho}$, then the density is written as

$$\rho(x,t) = \bar{\rho} + (\rho(x,t) - \bar{\rho}) \tag{4}$$

where $|\rho(x,t) - \bar{\rho}| \ll \bar{\rho}$ by assumption.

The forces on the fluid can be written as $\mathbf{F} = -g\mathbf{e}_z + \mathbf{D}$ where g is gravity and $\mathbf{D}$ is the external forces. The substitution of (4) and the equation of forces into (1) will give equation

$$\{\bar{\rho} + (\rho - \bar{\rho})\}\frac{D\mathbf{u}}{Dt} = -\nabla p - \{\bar{\rho} + (\rho - \bar{\rho})\}g\mathbf{e}_z + \{\bar{\rho} + (\rho - \bar{\rho})\}\mathbf{D} \tag{5}$$

Since $|\rho(x,t) - \bar{\rho}| \ll \bar{\rho}$, it is tempting to approximate the first term and last terms of the curly brackets by $\bar{\rho}$. The second term of the curly bracket is not approximate by $\bar{\rho}$ because the variations in density in combination with gravity lead to the buoyancy effect. The equation will reduces to

$$\frac{D\mathbf{u}}{Dt} = -\frac{1}{\bar{\rho}}\nabla p - \frac{\rho g}{\bar{\rho}}\mathbf{e}_z + \mathbf{D} \tag{6}$$

Suppose that $\mathrm{D} = 0$ and consider the presence of a uniform horizontal wind speed $\mathbf{u} = U\mathbf{e}_x$, where U is the background horizontal wind speed and $\mathbf{e}_x$ is unit vector in x-direction. By looking for two-dimensional disturbances of u', w', p' and ρ' to the flow of internal gravity waves, in which $u = U + u'(x,z,t)$, $w = 0 + w'(x,z,t)$, $p = p_0(z) + p'(x,z,t)$, and $\rho = \rho_0(z) + \rho'(x,z,t)$, the linearized equations of internal gravity waves in horizontal flow are obtained as follows.

$$\left(\frac{\partial}{\partial t} + U\frac{\partial}{\partial x}\right)u' = -\frac{1}{\bar{\rho}}\frac{\partial p'}{\partial x} \tag{7}$$

$$\left(\frac{\partial}{\partial t} + U\frac{\partial}{\partial x}\right)w' = -\frac{1}{\bar{\rho}}\frac{\partial p'}{\partial z} - \frac{g\rho'}{\bar{\rho}} \tag{8}$$

$$\frac{\partial u'}{\partial x} + \frac{\partial w'}{\partial z} = 0 \tag{9}$$

$$\left(\frac{\partial}{\partial t} + U\frac{\partial}{\partial x}\right)\rho' + w'\frac{\mathrm{d}\rho_0}{\mathrm{d}z} = 0 \tag{10}$$

By eliminating the variables p', u', and ρ' in equations (7-10), an equation which describes two-dimensional internal gravity waves in horizontal flow can be written as

$$\left(\frac{\partial^2}{\partial x^2} + \frac{\partial^2}{\partial z^2}\right)\left(\frac{\partial}{\partial t} + U\frac{\partial}{\partial x}\right)^2 w' + N^2(z)\frac{\partial^2 w'}{\partial x^2} = 0 \tag{11}$$

where $N(z)$ is known as buoyancy frequency and

$$N^2(z) = -\frac{g}{\bar{\rho}}\frac{\mathrm{d}\rho_0}{\mathrm{d}z} \tag{12}$$

The solution to the equation (11) is assume to be

$$w'(x,z,t) = \mathrm{Re}\left[\hat{w}\mathrm{e}^{i(kx+mz-\omega t)}\right] \tag{13}$$

Apply differentiation on (13) and follow by the substitution into (11) will yield the solution of

$$\mathrm{Re}\left[\left((k^2+m^2)(\omega - kU)^2 - N^2k^2\right)\left(\hat{w}\mathrm{e}^{i(kx+mz-\omega t)}\right)\right] = 0 \tag{14}$$

The variable $\hat{w}$ is suppose to be not equal to zero so that the solution is non-trivial. The manipulation of equation (14) can obtain the equation of dispersion relation, phase speed, and group velocity of internal gravity waves, which are

$$\omega = kU \pm \frac{Nk}{\sqrt{k^2+m^2}} \tag{15}$$

$$c_p = \frac{\omega}{k} = U \pm \frac{N}{\sqrt{k^2+m^2}} \tag{16}$$

$$\mathbf{c}_g = \left(\frac{\partial\omega}{\partial k}, 0, \frac{\partial\omega}{\partial m}\right) = \left(U \pm \frac{Nm^2}{(k^2+m^2)^{\frac{3}{2}}}, 0, \frac{\mp Nkm}{(k^2+m^2)^{\frac{3}{2}}}\right) \tag{17}$$

2.2 Mathematical Formulation under Topographic Features

The presence of topographic features such as hills will change the equation of internal gravity waves in horizontal flow. Suppose that the Earth's surface is deformed into an array of hills at $z = h'(x)$. The internal gravity waves will propagate upwards into the atmosphere and reach a steady state after a long time, which implies that $\partial/\partial t = 0$ as there is no time dependence. The equation in (11) will become

$$U^2\left(\frac{\partial^2}{\partial x^2} + \frac{\partial^2}{\partial z^2}\right)\frac{\partial^2 w'}{\partial x^2} + N^2(z)\frac{\partial^2 w'}{\partial x^2} = 0 \tag{18}$$

There is a boundary condition of no normal flow to be satisfied at the ground $z = h'(x)$. By writing $z - h'(x) = 0$ and normal vector $\mathbf{n} = \nabla\big(z - h'(x)\big) = (-\mathrm{d}h'/\mathrm{d}x, 0, 1)$, the boundary condition of w' in (18) can be obtained using

$$\mathbf{u} \cdot \mathbf{n} = 0 \tag{19}$$

By using linearization follow by Taylor series expansion at $z = h'(x)$, the corresponding boundary condition of w' is

$$w'(z = 0) = U\frac{dh'}{dx} \tag{20}$$

Now, consider the buoyancy frequency, N is constant, and $h' = \mathrm{Re}(\hat{h}\mathrm{e}^{ikx})$, where $\hat{h}$ is a complex number and $|\hat{h}|$ is the height of the hills, the solutions of w', which is the vertical velocity of waves is assume to be

$$w' = \mathrm{Re}(\widehat{w}(z)\mathrm{e}^{ikx}) \tag{21}$$

By differentiating w' in (21) with respect to x twice, follow by the substitution into (18) will obtain a second order ordinary differential equation as follow.

$$\frac{d^2\widehat{w}}{dz^2} + \left(\frac{N^2}{U^2} - k^2\right)\widehat{w} = 0 \tag{22}$$

with the boundary condition

$$\widehat{w}(z = 0) = ikU\hat{h} \tag{23}$$

The equation in (22) needs to be solved using the boundary condition in (23). In this study, the investigation will considers three distinct cases and the solutions are discussed in the following section.

3. Analytical Solutions

The solutions to the second order ordinary differential equation are solved using direct integration for case 1. For case 2 and case 3, it is solved using characteristic function.

Case 1 : $N^2 = k^2U^2$

The coefficient of $\widehat{w}$ is zero, so the most easiest way to solve the equation in (22) is by using direct integration. The corresponding solution is

$$\widehat{w} = ikU\hat{h} \tag{24}$$

Case 2 : $N^2 < k^2U^2$

For simplicity of the equation, a variable $\kappa = \sqrt{k^2 - (N^2/U^2)} \in \mathbb{R}^+$ is introduced in equation (22) and it is written as

$$\frac{d^2\widehat{w}}{dz^2} - \kappa^2\widehat{w} = 0 \tag{25}$$

By using the boundary condition in (23) and demanding that the solution remains finite as $z \to \infty$, the solution can be obtained as

$$\widehat{w} = ikU\hat{h}\mathrm{e}^{-\kappa z} \tag{26}$$

Case 3 : $N^2 > k^2U^2$

Similar as case 2, a variable $m = \sqrt{(N^2/U^2) - k^2} \in \mathbb{R}^+$ is introduced in equation (22) and it is written as

$$\frac{d^2\hat{w}}{dz^2} + m^2\hat{w} = 0 \tag{27}$$

By demanding the solution remains finite as $z \to \infty$ yields no new information since the solutions are sinusoidal. Therefore, by equating the coefficient of the decreasing function to zero, the constant values of the equation can be determined. Finally, the solution obtained is

$$\hat{w} = ikU\hat{h}\mathrm{e}^{imz} \tag{28}$$

4. Results and discussion

The expressions and graphical representations of the physical quantities of internal gravity waves for each case will be presented in this section. This section also discusses on the dispersion relation, phase speed, group velocity, and energy of waves in case 3.

4.1 Vertical Velocity

By using the expression of $\hat{w}$ obtained in previous section, the vertical velocity of internal gravity waves is calculated using (21). The solutions for each case are as follow.

$$\text{Case 1} : w' = kU\mathrm{Re}\left(i\hat{h}\mathrm{e}^{ikx}\right) \tag{29}$$

$$\text{Case 2} : w' = kU\mathrm{e}^{-\kappa z}\mathrm{Re}\left(i\hat{h}\mathrm{e}^{ikx}\right) \tag{30}$$

$$\text{Case 3} : w' = kU\mathrm{Re}\left(i\hat{h}\mathrm{e}^{i(kx+mz)}\right) \tag{31}$$

The vertical velocity profile of internal gravity waves are plotted using fix value of $\hat{h} = 200 + 50i$ with variations in horizontal wavenumber, k. The background horizontal wind speed, U and buoyancy frequency, N used in plotting the graphs are positive real numbers. The corresponding graphs are shown in Figure 1.

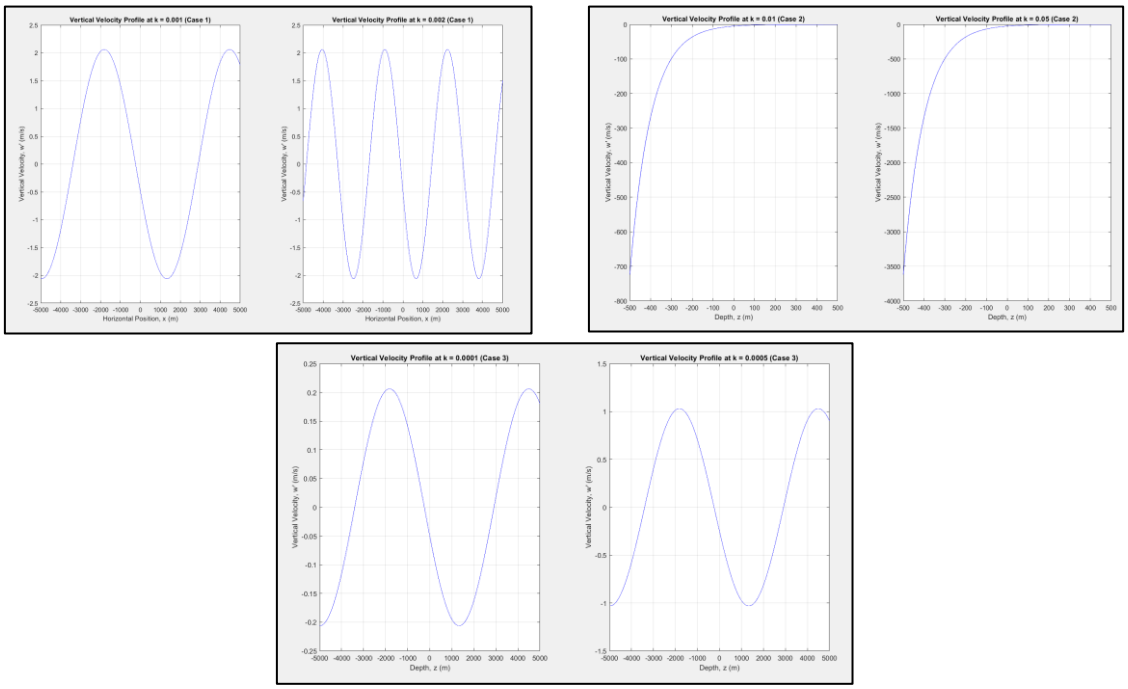

Figure 1 Vertical Velocity Profile for Internal Gravity Waves

The vertical velocity of internal gravity waves are vary sinusoidal for case 1 along the horizontal position. There are undulations above the hills as the vertical velocity changes when the waves pass over the hills. For case 2, the vertical velocity of waves decrease when the waves move deeper to the

hills. This situation occurred because the disturbances of waves are stronger at the surface as compared to the bottom of the hills. In contrast, the waves showed oscillations in the vertical velocity with respect to the depth for case 3. The phase of the waves are constant along the lines $kx + mz$. It is observed that the waves with lower horizontal wavenumber produces the graph with lower value of vertical velocity at wave-crests and troughs.

4.2 Horizontal Velocity

When the internal gravity waves move along the horizontal position, their horizontal velocity may changes due to the topographic features. By using the expression of vertical velocity, w', the corresponding horizontal velocity can be obtained using equation (9). The results from the calculations are as follow.

$$\text{Case 1} : u' = A \tag{32}$$

$$\text{Case 2} : u' = U\kappa \mathrm{e}^{-\kappa z}\mathrm{Re}\left(\hat{h}\mathrm{e}^{ikx}\right) \tag{33}$$

$$\text{Case 3} : u' = -mU\mathrm{Re}\left[i\hat{h}\mathrm{e}^{i(kx+mz)}\right] \tag{34}$$

The results showed that for case 1, the waves have constant value in horizontal velocity, which means that the speed and direction of flow remains the same at all points along the horizontal axis. For both case 2 and case 3, the analysis are done through graphical representations as shown in Figure 2.

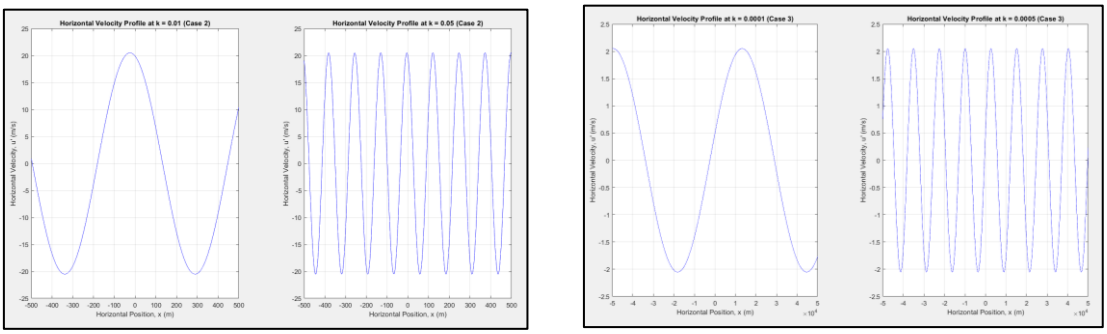

Figure 2 Horizontal Velocity Profile for Internal Gravity Waves

Based on Figure 2, both of the horizontal velocity of internal gravity waves vary sinusoidal with respect to the horizontal position. The use of higher horizontal wavenumber contributes to shorter wavelength, which results in higher frequency of waves. One of the differences between case 2 and case 3 is the wave-crests and troughs travel with smaller horizontal velocity in case 3 as compared to case 2.

4.3 Pressure

The propagation of waves have influence on the pressure. The changes of the pressure of waves are investigated as follow. By substituting u' into (7), the solutions for pressure for each case can be obtained as follow.

$$\text{Case 1} : p' = B \tag{35}$$

$$\text{Case 2} : p' = -\bar{\rho}U^2\kappa \mathrm{e}^{-\kappa z}\mathrm{Re}\left(\hat{h}\mathrm{e}^{ikx}\right) \tag{36}$$

$$\text{Case 3} : p' = \bar{\rho}mU^2\mathrm{Re}\left[i\hat{h}\mathrm{e}^{i(kx+mz)}\right] \tag{37}$$

Since horizontal velocity of internal gravity waves in case 1 is a constant value, therefore the pressure also remains as a constant value. It means that there is no variations in the pressure gradients of waves above topography. While for case 2 and case 3, there are variations in pressure gradient and the corresponding graphs are shown in Figure 3. The average density, $\bar{\rho} = 1025\ kg/m^3$ is used in plotting.

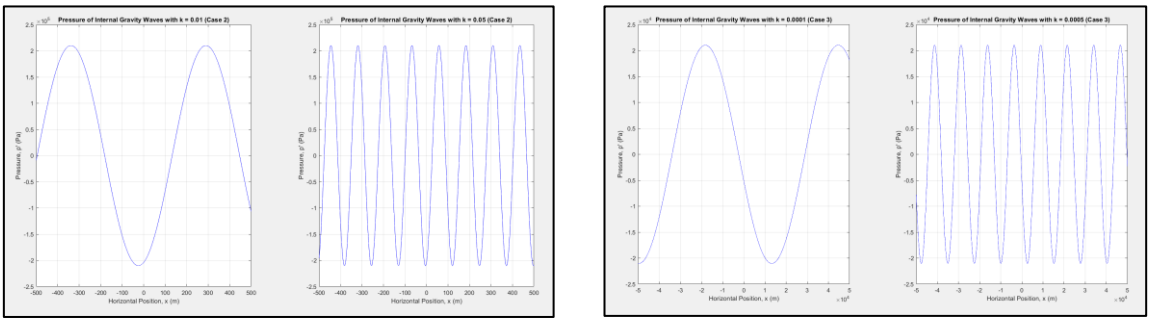

Figure 3 Pressure of Internal Gravity Waves

Based on Figure 3, the pressure of internal gravity waves in both cases show sinusoidal in variations. Both graphs show that higher horizontal wavenumber contributes to higher frequency of oscillations. From the analysis, it is observed that the pressure of internal gravity waves in case 3 are smaller as compared to case 2. This revealed that the pressure does not have significant effects on the waves propagation under case 3.

4.4 Density

As the internal gravity waves move up and down over the hills, the density will changes along the depth. Based on the obtained vertical velocity w', and pressure p', the expression of the density ρ', can be obtained by using the equation in (8). After the calculations, the corresponding expressions for density are shown below.

$$\text{Case 1}: \rho' = \frac{\bar{\rho}}{g} k^2 U^2 \mathrm{Re}\left(\hat{h} \mathrm{e}^{ikx}\right) \tag{38}$$

$$\text{Case 2}: \rho' = \frac{\bar{\rho}}{g} \left[U^2 (k^2 - \kappa^2) \mathrm{e}^{-\kappa z} \mathrm{Re}\left(\hat{h} \mathrm{e}^{ikx}\right)\right] \tag{39}$$

$$\text{Case 3}: \rho' = \frac{\bar{\rho}}{g} \left[U^2 (m^2 + k^2) \mathrm{Re}\left(\hat{h} \mathrm{e}^{i(kx+mz)}\right)\right] \tag{40}$$

The expressions of density involved a new variable, which is acceleration due to gravity, g. The value of g is fixed at $9.81\ ms^{-2}$ when plotting the graphs. The graphs are plotted using variations in horizontal wavenumber and are shown in Figure 4.

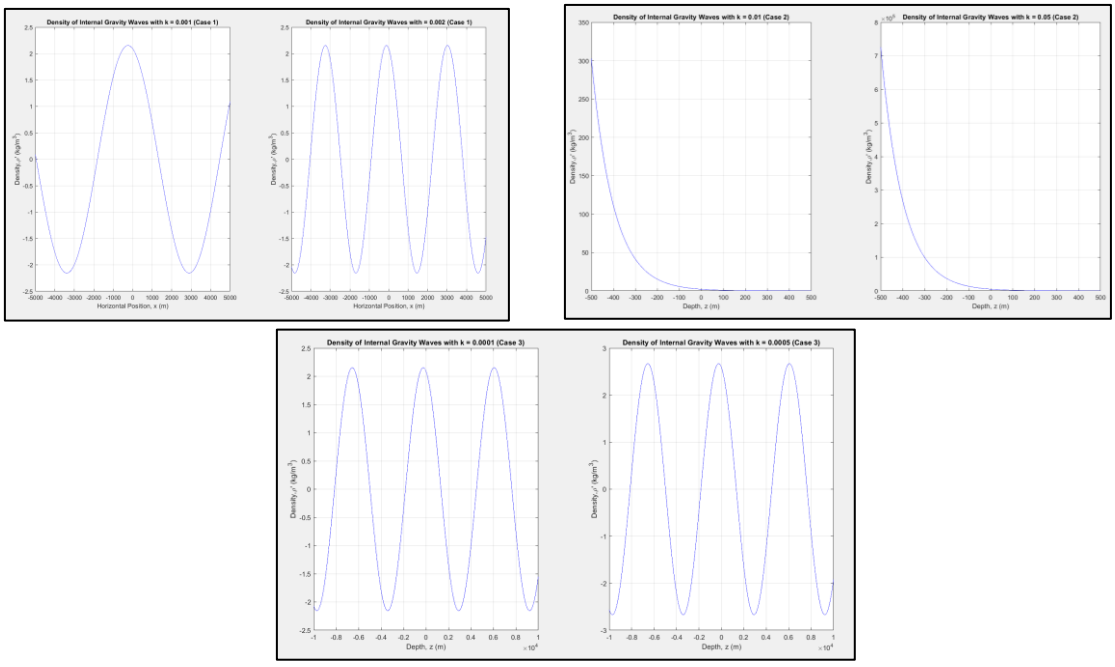

Figure 4 Density of Internal Gravity Waves

Since the density does not depend on the depth for case 1, therefore graphs of the density are plotted against the horizontal position. The graphs show that the density varies sinusoidal when the waves flow across x direction. When using higher horizontal wavenumber, the density show sharper waves at the crests and troughs. On the other hand, the density of waves are plotted with respect to the depth as it the density will varies depend on depth. For case 2, it is observed that the density decreases as the waves move near the surface of the hills. As the waves move deeper, the density tends to increase due to surrounding effects such as temperature and pressure. For case 3, the density are varies sinusoidal along the depth. The difference in horizontal wavenumber does not impacts on the period and frequency during the oscillation. It means that the waves have equal number of wave-crests and troughs independent of the horizontal wavenumber.

4.5 Dispersion Relation

The investigation of dispersion relation in (15) is important when analysing the behaviour of internal gravity waves when they propagate above the hills. For the purpose of investigation, the dispersion relation is set to be equal to zero. The manipulation of the equation will then obtained an equation for the variable, m, which is

$$m = \pm\sqrt{\frac{N^2}{U^2} - k^2} \tag{41}$$

This variable is known as vertical wavenumber. Based on observation, the solution of m obtained in (41) is consistent with the steady solution in case 3. It means that for case 3, the waves have zero frequency, as the dispersion relation is equal to zero. For the possibility of the dispersion relation to be equal to zero, it is necessary to take the negative sign in (15) as the background horizontal wind speed, U is assume to be positive. Therefore, the dispersion relation of internal gravity waves for case 3 can be written as

$$\omega = kU - \frac{Nk}{\sqrt{k^2+m^2}} \tag{42}$$

The equation in (42) shows that there exists a linear relationship between ω and k. To have better analysis on the dispersion relation, the corresponding graph is plotted using horizontal wavenumber from $k = 0.0001$ to $k = 0.0007$ and it is shown in Figure 5.

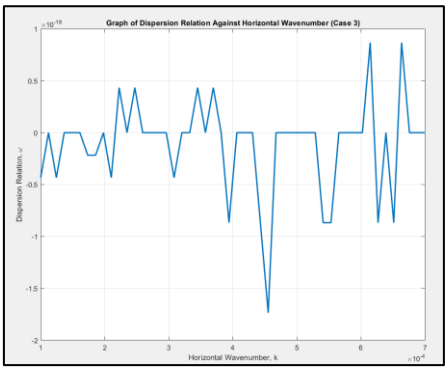

Figure 5 Graph of Dispersion Relation Against Horizontal Wavenumber

Although the dispersion relation is equal to zero, but the value shows slight deviations around the zero frequency line in Figure 5. The dispersion relation is not constant at zero along the line due to the influence of topographic features. When the waves interact with the topographic features, the waves undergo reflection and refraction, which leads to slightly changes in the dispersion relation.

4.6 Phase Speed

Based on the equation of dispersion relation in (42), an equation which describes the phase speed of

internal gravity waves for case 3 can be obtained by dividing ω with k. The result is shown below.

$$c_p = U - \frac{N}{\sqrt{k^2+m^2}} \tag{43}$$

Since the dispersion relation is approximate to zero, hence the phase speed also approximate to zero. To investigate the changes of phase speed around the zero line, the graph of phase speed against horizontal wavenumber is plotted and it is shown in Figure 6.

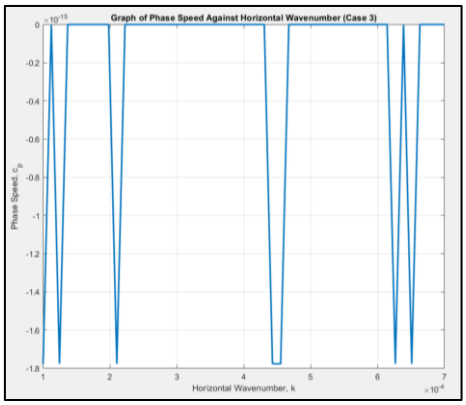

Figure 6 Graph of Phase Speed Against Horizontal Wavenumber

The graph in Figure 6 shows that the phase speed is slightly change below zero value. The negative phase speed means that the internal gravity waves propagate in the opposite direction to the background horizontal wind speed when they passes through the topographic features. The positive or negative slopes along the line indicate dispersive behaviour of the waves.

4.7 Group Velocity

The dispersion relation in (42) can be used to obtain the group velocities of internal gravity waves in x and z directions. The group velocity under case 3 can be written as follow.

$$\mathbf{c}_g = \left(\frac{\partial\omega}{\partial k}, 0, \frac{\partial\omega}{\partial m}\right) = \left(U - \frac{Nm^2}{(k^2+m^2)^{\frac{3}{2}}}, 0, \frac{+Nkm}{(k^2+m^2)^{\frac{3}{2}}}\right) \tag{44}$$

Based on (44), it indicates that the internal gravity waves have group velocity even though they have zero frequency. It means that the waves will transfer the energy when propagating. The graphs of group velocity vector field in both x and z directions are plotted in Figure 7 for analysis.

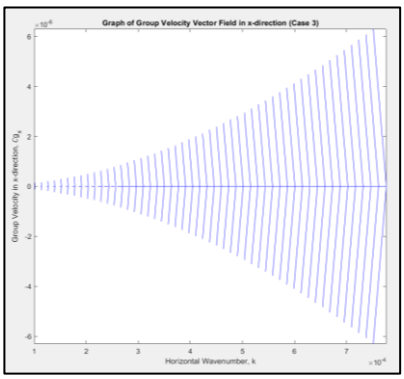

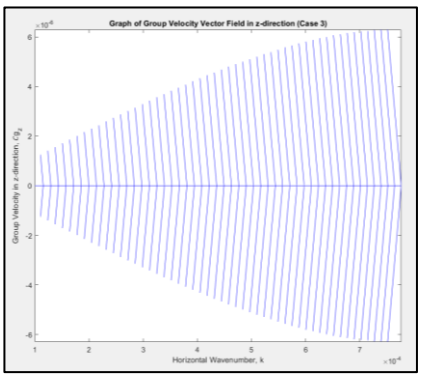

Figure 7 Graph of Group Velocity Vector Field in x and z directions

The graphs on Figure 7 shows that the vector arrows are increasing in sizes as the horizontal wavenumber increasing. The length of the vector arrows are longer in z-direction as compared to x-direction due to higher value of the magnitude of group velocity. The presence of background horizontal wind speed, U makes the waves propagate slowly along x-direction.

4.8 Energy of Internal Gravity Waves

The existence of group velocity tends to the existence of energy along the wave propagation. This is because the energy transferred by the group velocity. By using the linearized equations in (7-10), an equation describes the conservation law of internal gravity waves energy is obtained as follow.

$$\left(\frac{\partial}{\partial t} + U\frac{\partial}{\partial x}\right)E + \nabla \cdot \mathbf{J} = 0 \tag{45}$$

where E is the energy density and $\mathbf{J}$ is the vertical flux of energy. Their expressions are

$$E = \frac{1}{2}\bar{\rho}\left(u'^2 + w'^2\right) + \frac{g^2\rho'^2}{2\bar{\rho}N^2} \tag{46}$$

$$\mathbf{J} = p'(u', 0, w') \tag{47}$$

The graphical representations of internal gravity waves energy against depth are shown in Figure 8.

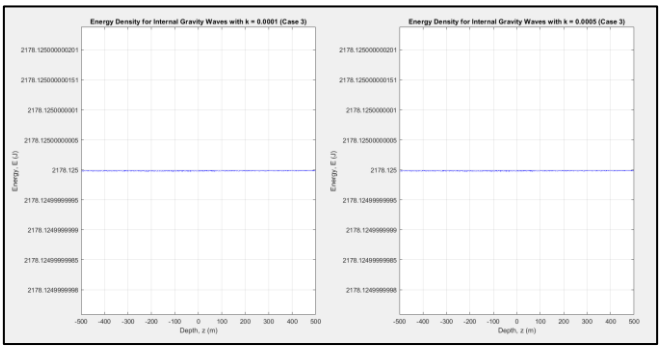

Figure 8 Graph of Energy Density for Internal Gravity Waves

The graphs in Figure 8 show that the energy density of internal gravity waves remain the same at $2178.125\,J$ for both horizontal wavenumber. This situation suggests that the energy density is independent of the horizontal wavenumber. The constant value of E means that the energy distribution of waves in uniform as the waves move up and down over the hills.

5. Conclusion

In this paper, the linearized partial differential equation in two-dimensions in the presence of topographic features of hills have been derived. The second order ordinary differential equation is solved for three distinct cases. Based on the solutions obtained, the physical quantities of internal gravity waves above topography for each cases are analysed using graphical representations. It is observed that each case show variations in the value of physical quantities based on variations in horizontal wavenumber. In case 3, where $N^2 > k^2U^2$, there is an observation of the absence of angular frequency when the waves propagate above hills, which resulting in an approximate zero phase speed. However, despite this absence, the internal gravity waves exhibited a group velocity as well as energy transfer. The vector arrows of group velocity are longer in z-direction as compared to x-direction. The graphs of energy density show that it is constant along the vertical axis. The energy distribution is uniform when the waves move within the fluid and it is independent of the horizontal wavenumber. In this study, the value of background horizontal wind speed, U and buoyancy frequency, N are treated as positive real numbers in analysis. Therefore, in future research, U can be treated as an oscillating function, while N can be treated as a function along the vertical axis. By implementing these recommendations, the precision of internal gravity waves model can be enhance significantly in future research.

Acknowledgement

I wish to express my sincere gratitude to all who have contributed throughout the course of this work.

References

[1] Rizal, S., Wafdan, R., Haditiar, Y., Ramli, M., & Halfiani, V. 2020. Numerical Study of Lee Waves

Characteristics in the Ocean. Journal of Engineering Science and Technology. 15(2): 1056-1078.
[2] Constantin, A. 2023. Exact nonlinear mountain waves propagating upwards. Journal of Physics A: Mathematical and Theoretical. 56(24).
[3] Lteif, R., & Khorbatly, B. 2022. Medium amplitude model for internal waves over large topography variation. Journal of Mathematical Analysis and Applications. 514(2).
[4] Durran, D.R. 2003. Lee Waves and Mountain Waves. Encyclopedia of Atmospheric Sciences: 1161-1169.

[5] Aguilar, D.A., Sutherland, B.R., & Muraki, D.J. 2006. Laboratory generation of internal waves from sinusoidal topography. Deep-Sea Research II: Tropical Studies in Oceanography. 53(1-2): 96-115.
[6] Draxl, C., Worsnop, R.P., Xia, G., Pichugina, Y., Chand, D., Lundquist, J.K., Sharp, J., Wedam, G., Wilczak, J.M., & Berg, L.K. 2021. Mountain waves can impact wind power generation. Wind Energy Science. 6(1): 45-60.
[7] Heale, C.J., Bossert, K., Vadas, S.L., Hoffmann, L., Dörnbrack, A., Stober, G., Snively, J.B., & Jacobi, C. 2020. Secondary Gravity Waves Generated by Breaking Mountain Waves Over Europe. Journal of Geophysical Research: Atmospheres. 125(5).
[8] Zeytounian, R.K. 2003. Joseph Boussinesq and his approximation: a contemporary view. Comptes Rendus Mecanique. 331(8): 575-586.
[9] Bulatov, V., & Vladimirov, Y. 2020. Generation of Internal Gravity Waves Far from Moving Non-Local Source. Symmetry. 12(11).
[10] Bulatov, V.V., Vladimirov, Y.V., & Vladimirov, I.Y. 2021. Phase Structure of Internal Gravity Waves in the Ocean with Shear Flows. Journal of Physical Oceanography. 28(4): 438-453.
[11] Liu, Z., Han, P., Fang, K., & Liu, Y. 2023. A high-order nonlinear Boussinesq-type model for internal waves over a mildly-sloping topography in a two-fluid system. Ocean Engineering. 285(1).
[12] Chesnokov, A.A., Gavrilyuk, S.L., & Liapidevskii, V.Y. 2021. Long nonlinear internal waves and mixing in a three-layer stratified flow in the Boussinesq approximation. Journal of Fluid Mechanics.
[13] Charlier, C., & Lenells, J. 2023. On Boussinesq's equation for water waves. Mathematical Physics.
[14] Eden, C., Pollmann, F., & Olbers, D. 2019. Numerical Evaluation of Energy Transfers in Internal Gravity Wave Spectra of the Ocean. Journal of Physical Oceanography. 49: 737-749.
[15] Stashchuk, N., & Vlasenko, V. 2022. Energetics of tidally induced internal waves over isolated seamount. Wave Motion. 114.
[16] Hakes, K., & Crockett, J. 2020. Internal Waves Generated from Asymmetric Topographies. Conferences and Events.
[17] Hu, Q., Huang, X., Zhang, Z.W., Zhang, X.J., Xu, X., Sun, H., Zhou, C. Zhao, W., & Tian, J. 2020. Cascade of Internal Wave Energy Catalyzed by Eddy-Topography Interactions in the Deep South China Sea. Geophysical Research Letters. 47(4).
[18] Shcherbina, A.Y., Talley, L.D., Firing, E., & Hacker, P. 2003. Near-Surface Frontal Zone Trapping and Deep Upward Propagation of Internal Wave Energy in the Japan/East Sea. Journal of Physical Oceanography. 33: 900-912.
[19] Khatiwala, S. 2003. Generation of internal tides in an ocean of finite depth: analytical and numerical calculations. Deep Sea Research Part I: Oceanographic Research Papers. 50(1): 3-21.
[20] Lenain, L., & Pizzo, N. 2021. Modulation of Surface Gravity Waves by Internal Waves. Journal of Physical Oceanography. 51: 2735-2748.
[21] Gill, A.E. 1982. Atmosphere-Ocean Dynamics. Retrieved from https://archive.org/details/AtmosphereOceanDynamicsGill/page/n3/mode/2up
[22] Voelker, G.S., Myers, P.G., Walter, M., & Sutherland, B.R. 2019. Generation of oceanic internal gravity waves by a cyclonic surface stress disturbance. Dynamics of Atmospheres and Oceans.

86: 116-133.
[23] Ratnasingam, R.P., Edelmann, P.V.F., & Rogers, T.M. 2020. Two-dimensional simulations of internal gravity waves in the radiation zones of intermediate-mass stars. Monthly Notices of the Royal Astronomical Society. 497(4): 4231-4245.
[24] Fan, C.M,, Chu, C.N., Sarler, B., & Li, T.H. 2019. Numerical solutions of waves-current interactions by generalized finite difference method. Engineering Analysis with Boundary Elements. 100: 150-163.
[25] Bajars, J., Frank, J., & Maas, L.R.M. 2013. On the appearance of internal wave attractors due to an initial or parametrically excited disturbance. Journal of Fluid Mechanics. 714: 283-311.
[26] Shi, F., Dalrymple, R.A., Kirby, J.T., Chen, Q., & Kennedy, A. 2001. A fully nonlinear Boussinesq model in generalized curvilinear coordinates. Coastal Engineering. 42(4): 337-358.
[27] Johnston, T.M.S., & Merrifield, M.A. 2003. Internal tide scattering at seamounts, ridges, and islands, Journal of Geophysical Research: Oceans. 108(C6).
[28] Rizal, S., Iskandar, T., Muhammad, Haditiar, Y., Ilhamsyah, Y., Setiawan, I., & Sofyan, H. 2019. Numerical Study of the Internal Wave Behaviour in the Vertical Ocean Slice Model. Journal of Engineering Science and Technology. 14(5): 2836-2846.
[29] Veremieiev, S., Thompson, H.M., & Gaskell, P.H. 2015. Free-surface film flow over topography: Full three-dimensional finite element solutions. Computers & Fluids. 122: 66-82.
[30] Zou, P.X., Bricker, J.D., & Uijttewaal, W.S.J. 2021. The impacts of internal solitary waves on a submerged floating tunnel. Ocean Engineering. 238.
[31] Shara, S.N., Birk, C., & Gravenkamp, H. 2023. Efficient simulation of waves in heterogeneous domains using the scaled boundary finite element method. Proceedings in Applied Mathematics & Mechanics. 22(1).
[32] Duffin, C., Cripps, E., Stemler, T., & Girolami, M. 2020. Statistical finite elements for misspecified models. Physical Sciences. 118(2).
[33] Phadke, A.C., & Cheung, K.F. 2001. Resonance and response of fluid-filled membrane in gravity waves. Applied Ocean Research. 23(1): 15-28.
[34] Vukčević, V., Roenby, J., Gatin, I., & Jasak, H. 2018. A Sharp Free Surface Finite Volume Method Applied to Gravity Wave Flows. Journal of Computational Physics.
[35] Qwist, J.R.K., & Christensen, E.D. 2022. Solitary Wave Propagation Using a Novel Single Fluid Finite Volume Method for Free Surface Gravity Waves. Proceedings of the ASME 2022: 41st International Conference on Ocean, Offshore and Arctic Engineering. 7.
[36] Bourdarias, C., Gerbi, S., & Lteif, R. 2017. A numerical scheme for an improved Green-Naghdi model in the Camassa-Holm regime for the propagation of internal waves. Computers & Fluids. 156: 283-304.
[37] Paskyabi, M.B., & Fer, I. 2012. Upper Ocean Response to Large Wind Farm Effect in the Presence of Surface Gravity Waves. Energy Procedia. 24: 245-254.
[38] Fringer, O.B., Gerritsen, M., & Street, R.L. 2006. An unstructured-grid, finite-volume, nonhydrostatic, parallel coastal ocean simulator. Ocean Modelling. 14(3-4): 139-173.
[39] Matsuura, T., & Hibiya, T. 1990. An Experimental and Numerical Study of the Internal Wave Generation by Tide-Topography Interaction. Journal of Physical Oceanography. 20: 506-521.
[40] Lim, K., Ivey, G.N., & Jones, N.L. 2010. Experiments on the generation of internal waves over continental shelf topography. Journal of Fluid Mechanics. 663: 385-400.
[41] Sandstrom, H. 1966. The Importance of Topography in Generation and Propagation of Internal Waves [Doctoral dissertation, University of California]. ProQuest Dissertations & Theses Global.
[42] Caldwell, D.R., Brubaker, J.M., & Neal, V.T. 1978. Thermal microstructure on a lake slope 1. Limnology and Oceanography. 23(2): 372-374.
[43] Sutton, R.F., & Dalziel, S.B. 2011. Internal wave attractors without sloping boundaries. Journal of Physics: 22-26.
[44] Maas, L.R.M., Benielli, D., Sommeria, J., & Lam, F.A. 1997. Observational of an internal wave

attractor in a confined, stably stratified fluid. Journal of Nature. 388: 557-561.
[45] Hazewinkel, J., Grisouard, N., & Dalziel, S.B. 2011. Comparison of laboratory and numerically observed scalar fields of an internal wave attractor. European Journal of Mechanics B/Fluids. 30(1): 51-56.
[46] Klemp, J.B., Lilly, D.K. 1978. Numerical Simulation of Hyrostatic Mountain Waves. Journal of the Atmospheric Sciences. 35: 78-107.
[47] Xu, X., Shu, S., & Wang, Y. 2017. Another look on the structure of mountain waves: A spectral perspective. Atmospheric Research. 191: 156-163.
[48] Bouruet-Aubertot, P., & Thorpe, S.A. 1999. Numerical experiments on internal gravity waves in an accelerating shear flow. Dynamics of Atmospheres and Oceans. 29(1): 41-63.

[49] Sree, D.K.K., Law, A.W., & Shen, H.H. 2020. An experimental study of gravity waves through segmented floating viscoelastic covers. Applied Ocean Research. 101.
[50] Slinn, D.N., & Riley, J.J. 1996. Turbulent mixing in the oceanic boundary layer caused by internal wave reflection from sloping terrain. Dynamics of Atmospheres and Oceans. 24(1-4): 51-62.
[51] Constantin, A. 2001. On the deep water wave motion. Journal of Physics A: Mathematical and General. 34(7): 1405-1417.
[52] Sabatini, R., Snively, J.B., Bailly, C., Hickey, M.P., & Garrison, J.L. 2019. Numerical Modeling of the Propagation of Infrasonic Acoustic Waves Through the Turbulent Field Generated by the Breaking of Mountain Gravity Waves. Geophysical Research Letters. 46(10): 5526-5534.
[53] Ismail, N.N.N.N., Alias, A., & Harun, F.N. 2020. The Propagation of Nonlinear Internal Waves under the Influence of Variable Topography and Earth's Rotation in a Two-Layer Fluid. Fluids. 5(3): 140.
[54] Zhanbirova, G., Zavyalova, G., Muraveva, E., & Shabdirov, D. 2021. Modeling internal waves in a two-layer fluid flow. E3S Web of Conferences. 288(2).
[55] Bouruet-Aubertot, P., Sommeria, J., & Staquet, C. 1996. Stratified turbulence produced by internal wave breaking: two-dimensional numerical experiments. Dynamics of Atmospheres and Oceans. 23(1-4): 357-369.
[56] Pan, Y., Arbic, B.K., Nelson, A.D., Menemenlis, D., Peltier, W.R., Xu, W., & Li, Y. 2020. Numerical Investigation of Mechanisms Underlying Oceanic Internal Gravity Wave Power-Law Spectra. Journal of Physical Oceanography. 50: 2713-2733.